

# Three-dimensional relativistic MHD simulations of bow shock nebulae

B. Olmi<sup>1,2</sup> and N. Bucciantini<sup>2,3,4</sup>

<sup>1</sup> Istituto Nazionale di Astrofisica (INAF) – Osservatorio Astronomico di Palermo, Piazza del Parlamento 1, 90134 Palermo, Italy, e-mail: [barbara.olmi@inaf.it](mailto:barbara.olmi@inaf.it)

<sup>2</sup> Istituto Nazionale di Astrofisica (INAF) – Osservatorio Astrofisico di Arcetri, Largo Enrico Fermi 5, 50125 Firenze, Italy

<sup>3</sup> Università degli Studi di Firenze – Dipartimento di Fisica e Astronomia, Via G. Sansone 1, 50019 Sesto Fiorentino (FI), Italy

<sup>4</sup> Istituto Nazionale di Fisica Nucleare (INFN) – Via G. Sansone 1, 50019 Sesto Fiorentino (FI), Italy

**Abstract.** Bow shock pulsar wind nebulae have been observed with diverse morphologies, both when comparing the same source at different wavelengths or when looking at different objects. Different conditions of the surrounding medium or properties of the pulsar wind have been generally invoked as possible causes of these diversities. Here we have investigated a large set of physical conditions of such systems by means of 3D relativistic MHD numerical simulations. A good coverage of the parameters space describing different conditions of the pulsar wind at injection is ensured with the variation of the most representative parameters: the level of magnetization, the latitudinal anisotropy of the wind energy flux, the inclination of the pulsar spin axis with respect to the star direction of motion. We have investigated the dynamics of the resulting bow shock nebulae and their tails, detailed the onset of turbulence and the effects on the emitting properties.

**Key words.** ISM: supernova remnants – ISM: cosmic rays – magnetic fields – MHD – methods: numerical – pulsars: general

## 1. Introduction

Results obtained with the present project (INA17\_C2A14, 4 millions of cpu hours) are published in [Olmi & Bucciantini 2019a,b](#). This project has a follow-up, in which we have studied the escape of particles from bow shock nebulae (INA17\_C4A31), whose results are discussed in [Olmi & Bucciantini 2019c](#). The MoU INAF–CINECA agreement made possible to get important numerical resources with a dedicated and simple submission form, with a rapid evaluation of the projects and accessibil-

ity of allocated time. Bow shock pulsar wind nebulae (BSPWNe) are one of the manifestations of the pulsar wind nebulae (PWNe) family. PWNe are produced by the wind emanating from a pulsar as a consequence of its spin-down process. Bow shocks are in particular associated with evolved systems, with age  $\gtrsim 20000$  years. It has been estimated that a relevant fraction of all the pulsars (10 – 50%) was born with an high kick velocity, of order 100–500 km/s. On the contrary, supernova ejecta are in decelerated expansion in the sur-

rounding interstellar medium (ISM). Most of the pulsars are thus fated to escape their supernova remnant shell on timescales shorter than their typical ages. As soon as the pulsar is escaped its progenitor shell, it starts to interact directly with the ISM. Since the typical sound speed in the ISM is well lower than the pulsar kick velocity ( $c_s \sim 10 - 100$  km/s), the pulsar motion becomes suddenly supersonic. This strongly modifies the PWN morphology: a bow shock forms around the nebula, shaping it in a cometary-like fashion, with the pulsar located at the head of an elongated nebula, with a very extended tail following the pulsar. Many bow shock nebulae have been observed as sources of non-thermal radiation in the radio or X-ray bands (Kargaltsev & Pavlov 2008; Brownsberger & Romani 2014). For a few objects also polarimetric information are available, suggesting a large variety of magnetic configurations both in the head and in the tail. Recently multi-frequency observations have revealed very complex emission patterns, with variable morphologies of the tail, misaligned jets (extending in the orthogonal direction with respect to the direction of motion of the star) and the presence of extended TeV halos surrounding the bow shock. This very large and complex phenomenology is not completely understood yet. A better comprehension of the physics of those systems would also have important consequences for fundamental physics, from relativistic plasma physics to the physics of pulsar magnetospheres. Bow shock nebulae have been also revealed in  $H_\alpha$ , making them the perfect systems to look at for studying the interaction of relativistic plasmas and partially ionized media.

## 2. Simulations and results

Given the complexity of BSPWNe and the non-symmetric properties they show, a complete modelling requires a full 3D approach. Our simulations have been performed with the numerical code PLUTO (Mignone et al. 2007), using the Adaptive Mesh Refinement (AMR) facility to increase numerical resolution where needed (Mignone et al. 2012). The physical scales of the system are in fact extremely dif-

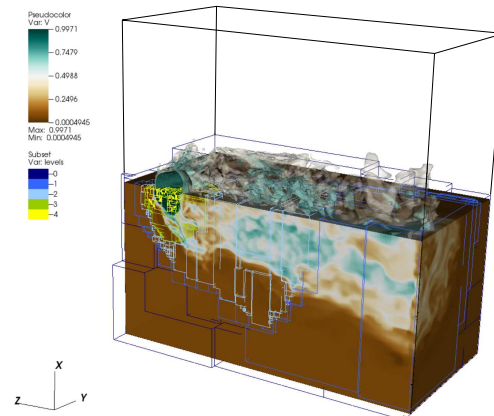


**Fig. 1.** Pseudocolor plot of the velocity magnitude in the bow shock, for a selected configuration, with the anisotropic TS shown in emerald color. Boundary of AMR boxes are shown with the color-coded scale shown on the left side of the image (figure taken from Olmi & Bucciantini 2019a).

ferent – approximately 3 orders of magnitude from the region of injection of the pulsar wind to the bow shock tail – and a static grid cannot properly account for the required resolution at the domain center or, otherwise, will require an enormous amount of resources.

The numerical setup was optimized during the test phase of the project: we have defined the optimal numerical methods, the grid extension and base level, the number of AMR levels to be used in order to achieve the requested resolution at the injection region. To reduce as much as possible the numerical requirements, AMR levels are activated only in specific sectors of the numerical domain. In order to manage the relativistic wind we have modified the standard conditions of the Riemann solver, by relaxing the HLLD solver to the HLL one in all the relativistic regions. This allows for using an high Lorentz factor ( $\gamma = 10$ ), ensuring the code to remain stable. The cartesian domain has been defined such as the pulsar is located at the grid origin, with the direction of motion along the  $z$  axis. For simplicity the grid is chosen to be comoving with the pulsar, so that the pulsar is at rest at the domain center and sees the uniform, unmagnetized, ISM moving in its

direction (with velocity along  $-z$ ). The domain extends between  $[-17d_0, +17d_0]$  along the  $x$  and  $y$  directions and between  $[-28d_0, +5d_0]$  along the  $z$  one, where the bow shock tail is expected to form (the grid configuration can be seen in Fig. 1) Distances have been defined in terms of the characteristic bow shock parameter, the so called *stand-off distance*:

$$d_0 = \sqrt{L/(4\pi c \rho_{\text{ISM}} v_{\text{PSR}}^2)}, \quad (1)$$

where  $L$  is the pulsar spin-down luminosity,  $\rho_{\text{ISM}}$  the ISM density,  $v_{\text{PSR}}$  the pulsar velocity and  $c$  the speed of light. The base grid is made of  $128^3$  monospaced cells and 4 AMR levels have been used to reach the maximum equivalent resolution of  $2048^3$  cells. We have verified this to be enough to ensure the required resolution at the wind injection ( $r < 0.2d_0$ ), the correct evolution of the wind termination shock (TS) and for resolving properly the highly dynamical region of the head.

To investigate the observed variety of morphology of BSPWNe we have studied a large set of models, varying in particular the physical parameters which we expect could mostly affect the final shape of the bow shock. We have considered thus 4 different levels of the wind magnetization (from non-magnetized to highly magnetized, with the magnetization parameter being  $\sigma = [0, 0.01, 0.1, 1]$ ), different inclination angles between the pulsar spin-axis and the direction of motion ( $0^\circ, 45^\circ, 90^\circ$ ) and also different models for the pulsar wind, considered either isotropic (with the energy flux isotropically distributed in the wind) or anisotropic (with most of the energy flux concentrated along the pulsar equatorial plane).

We found that the large scale structure of the bow shock is quite similar from case to case, with major deviations due to the inclination of the pulsar spin-axis with respect to the direction of motion. Variations of the magnetization lead to evident differences in the development of turbulence, as can be seen in Fig. 2 low magnetized cases are characterized by very strong turbulence at small scales, producing a high mixing of the flow in the tail and a consequent strong magnetic dissipation. Injection conditions are lost immedi-

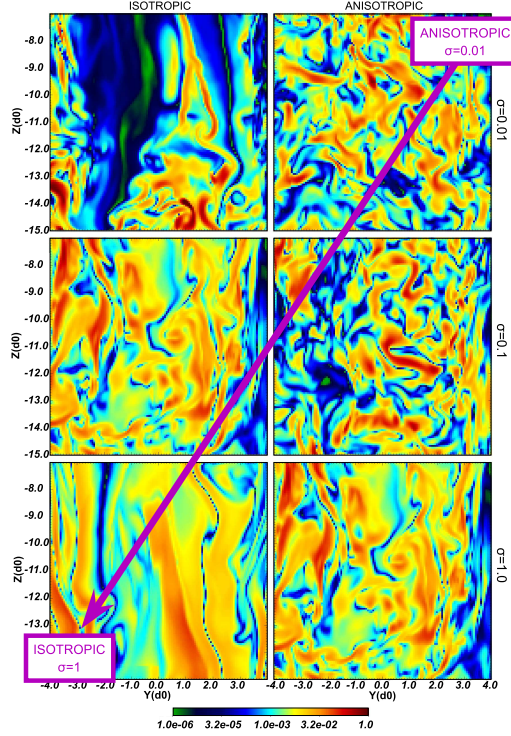


**Fig. 2.** 2D slices of the magnetization in the tail, with the appropriate definition for a relativistic gas  $B^2/(4p + \rho)$  in the region in the bow shock tail defined by  $z \in [-15, -7]d_0$ ,  $y \in [-4, 4]d_0$ , and  $x = 0$  and for a  $45^\circ$  inclination of the spin-axis. Left-side column shows images for the isotropic models, right-side column the anisotropic models. Magnetization changes from top to bottom. Maps are normalized to their respective maxima (from the lowest to the highest  $\sigma$  0.3, 0.9, 1.8 for the isotropic cases, and 0.8, 0.3, 1.6 for the anisotropic ones). From the upper-right panel to the bottom-left one the models change behavior from highly turbulent with complete loss of injection information, to lowly turbulent with a quasi-laminar flow that maintains the injection information. This behavior follows the direction indicated by the violet arrow.

ately behind the TS. The tail is characterized by small structures and a low magnetic field, which has been completely randomized. This effect is particularly evident in anisotropic models, which show the highest level of turbulence at the same value of magnetization, with the most turbulent being the one with in-

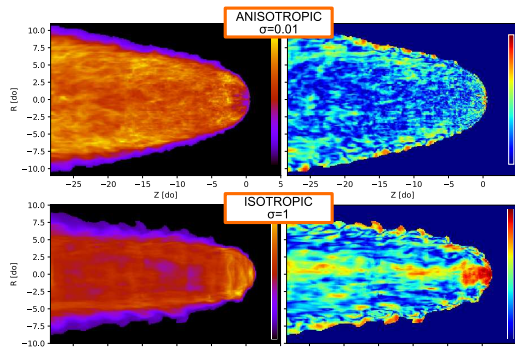


**Fig. 3.** Surface brightness and polarization level maps for the two extreme cases: anisotropic and low magnetized (upper panel), isotropic and highly magnetized (lower panel). All the maps are normalized to the maximum. Figures are taken from [Olmi & Bucciantini \(2019b\)](#).

clination  $45^\circ$  and  $\sigma = 0.01$ . As magnetization increases, the injection properties of the wind are slowly recovered. Finally the high magnetized case, with isotropic wind, shows a quasi-laminar structure of the flow in the entire tail, with the magnetic field well structured and still high far away from the pulsar location, meaning that now magnetic dissipation is not very efficient.

This complex variability of the bow shock tail depending on the wind model, the level of magnetization and the consequent development of small-scale turbulence, has strong consequences on the observed properties of the source. Anisotropic models with low magnetization – highly turbulent – show a rather uniform emissivity and no polarization (see [Fig. 3](#)). On the contrary isotropic models with high magnetization – no turbulence – have an head-dominated emission and a strong polarization.

With the present project we have studied in a full-3D approach the dynamical and emissivity properties of bow shock pulsar wind nebulae. We have identified the most important physical parameters, connecting different morphologies of the sources to different sets of

them, and isolating the effects of each one. We have in particular shown that only in the case of high magnetization the structure of the flow in the tail stays quasi-laminar, as expected from simplified analytical models ([Bucciantini 2018](#)), also maintaining the information of its injection properties (i.e. keeping trace of the pulsar physics). The most of the models show the development of a very high degree of turbulence in the entire tail, which tends to destroy completely the injection structure of the wind and to dissipate large part of the magnetic field, having evident consequences on the degree of polarization and uniformity of emission.

*Acknowledgements.* The authors acknowledge financial support from the “*Accordo Attuativo ASI-INAF n. 2017-14-H.0 Progetto: on the escape of cosmic rays and their impact on the background plasma*” and from the INFN Teongrav collaboration.

We acknowledge the computing centre of Cineca and INAF, under the coordination of the “*Accordo Quadro MoU per lo svolgimento di attività congiunta di ricerca Nuove frontiere in Astrofisica: HPC e Data Exploration di nuova generazione*”, for the availability of computing resources and support.

## References

- Brownsberger, S., Romani, R. W. 2014, *ApJ*, 784, 154
- Bucciantini, N. 2018, *MNRAS*, 480, 5419
- Kargaltsev, O., Pavlov, G. G. 2008, in *40 Years of Pulsars: Millisecond Pulsars, Magnetars and More*, ed. C. Bassa, Z. Wang, A. Cumming, & V. M. Kaspi (AIP, Melville, N.Y.), *AIP Conf. Proc.*, 983, 171
- Mignone, A., et al. 2007, *ApJS*, 170, 228
- Mignone, A., et al. 2012, *ApJS*, 198, 7
- Olmi, B., Bucciantini, N. 2019a, *MNRAS*, 484, 5755
- Olmi, B., Bucciantini, N. 2019b, *MNRAS*, 488, 5690
- Olmi, B., Bucciantini, N. 2019c, *MNRAS*, 490, 3608